Isolating Reactions at the Picoliter-scale: Parallel Control of Reaction Kinetics at the Liquid-liquid Interface**

*Gia Chuong Phan-Quang, Hiang Kwee Lee, Xing Yi Ling**

Abstract: *Miniaturized liquid-liquid interfacial reactors offer enhanced surface area and rapid confinement of compounds of opposite solubility, yet unable to provide in-situ molecular-level reaction monitoring at the interface. Here we utilize plasmonic colloidosomes with Ag octahedra strategically assembled at the water-in-decane emulsion surface as a pico-reactor to perform reactions at the liquid-liquid interface. Our plasmonic colloidosomes can isolate ultrasmall amount of <200 pL solutions, for parallel monitoring of multiple reactions simultaneously. We are also able to in-situ monitor the interfacial protonation of dimethyl yellow via SERS technique, which elucidates the apparent rate constant at 0.09 min^{-1} of this first-order reaction. We also resolve the presence of structural-isomeric products of similar physical properties, which is otherwise indiscernible by other analytical method.*

Colloidosomes are robust spherical microcapsules formed via the self-assembly of nanoparticles onto immiscible liquid-liquid interface during emulsification.[1] They inherit the characteristics of an emulsion system, including dual-phase nature, large surface area and remarkable interfacial stability.[2] They can be imparted with additional functionality via the choice of nanoparticles used.[3] Notably, an attractive application of colloidosomes is their use as liquid-liquid interfacial picoreactors,[4] due to their unique confinement of multiple reagents of opposite solubility within close proximity at their permeable shells.[4b, 5] Furthermore, the enhanced interfacial area of such picoreactors facilitates diffusion-limited phase transfer of molecules across an interface,[4b] and improves interfacial reaction efficiency by tens of order of magnitude compared to macroscopic systems.[2, 6] However, a major drawback of current colloidosome reactors is their reliance on *ex-situ* monitoring techniques which could not offer vital molecular information.[7] Consequently, it is not possible to study the intrinsic reaction dynamic and differentiation of physically-similar isomeric species at its native biphasic environment.

Plasmonic colloidosomes constructed from noble metal nanoparticles are excellent three-dimensional (3D) surface-enhanced Raman spectroscopy (SERS) platforms that tackle the aforementioned limitations.[8] Equipped with high density of intense SERS hot spots, ultrasensitive plasmonic colloidosomes provide specific molecular vibrational fingerprints simultaneously across the immiscible liquids.[8] Their ability to compartmentalize various liquids creates immense potential as a pico-scale reactor for parallel reaction screening.[7, 9] Most importantly, they enable *in-situ* tracking of molecular events directly at the native liquid-liquid interface, which is crucial for elucidating reaction kinetics and mechanism,[10] and ultimately allows the discovery and optimization of new reaction pathways in synthetic chemistry.[11]

Herein, we fabricate Ag octahedra-stabilized plasmonic colloidosome to confine picoliter of liquids for parallel reaction kinetics control of multiple liquid-liquid interfacial reactions. Our model reaction is the interfacial protonation of dimethyl across the decane-water interface. Together with computational density functional theory (DFT) simulation, our *in-situ* SERS highlights the successful differentiation and quantification of two unprecedented isomeric products, exemplifying the superiority of plasmonic colloidosome over conventional high performance liquid chromatography (HPLC) technique in resolving physically-similar isomers. Correspondingly, the reaction order and its kinetics are determined based on the consumption of H^+ protons over trials with multiple pH values, which exemplifies the excellent quantitative SERS capability of plasmonic colloidosome. The high through-put monitoring of interfacial reaction is also demonstrated on multiple colloidosomes placed in a single organic phase.

Ag octahedra nanoparticles of (350 ± 40) nm (Figure S1) are used as encapsulating solids for the fabrication of plasmonic colloidosomes due to their highly efficient light scattering effect.[12] Colloidosomes are prepared by intense emulsification of micro-liter aqueous droplet in colloidal decane suspension of hydrophobic perfluorodecanethiol-grafted Ag octahedra (Figure 1A). The as-formed spherical colloidosomes exhibit an average diameter of (72 ± 20) µm (Figure 1B) with closely-packed plasmonic shells comprising of (5 ± 1) layers of Ag octahedra (Figure 1C, D). Furthermore, plasmonic colloidosomes demonstrate the strongest SERS activities at their Ag shell which is capable of sensing methylene blue down to ~ 20 attomole level (Figure 1E-G), corresponding to an analytical enhancement factor of 10^5 (Figure S2, supporting information 1). This is attributed to the high density of intense SERS hot spot arising from closely-packed Ag octahedra clusters across the colloidosome's three-dimensional (3D) surface. Due to their size-independent SERS sensitivity, from hereon, we use plasmonic colloidosomes of diameter (72 ± 20) µm, corresponding to ~ 195 pL, for our latter reaction control and study.[8]

We use plasmonic colloidosome to conduct a miniaturized interfacial protonation of dimethyl yellow (DY) at the decane-water interface (Figure 2), to demonstrate its dual-functionality as a permeable picoreactor for liquid-liquid interfacial reaction and also an *in-situ* SERS monitoring platform. The reaction generally involves the protonation of organic-soluble DY (yellow; in decane) into aqueous-soluble protonated dimethyl yellow (red; HDY^+) at the interface, followed by the diffusion of HDY^+ into the encapsulated aqueous phase (Figure S3A). It is also noteworthy that the interfacial protonation of DY happens only at pH values lower than their pKa value of 3.3.[13] Such interfacial protonation reactions are important and widely applied as a separation technique to extract organic molecules from organic phase into aqueous phase for purification or latter characterization.[14] However, there has been no report on the

[*] G.C. Phan-Quang, H. K. Lee, Prof. X. Y. Ling
Division of Chemistry and Biological Chemistry, School of Physical and Mathematical Sciences, Nanyang Technological University
50 Nanyang Avenue, Singapore 637371
E-mail: xyling@ntu.edu.sg

H. K. Lee
Institute of Materials Research and Engineering
Agency for Science, Technology and Research (A*STAR)
2 Fusionopolis Way, Innovis, #08-03, Singapore 138634

[**] X.Y.L. thanks Singapore National Research Foundation (NRF-NRFF2012-04) for support. G.C.P.-Q acknowledges the support from Nanyang Presidential Graduate Scholarship. H.K.L thanks the A*STAR graduate scholarship from A*STAR, Singapore.

Supporting information for this article is given via a link at the end of the document.

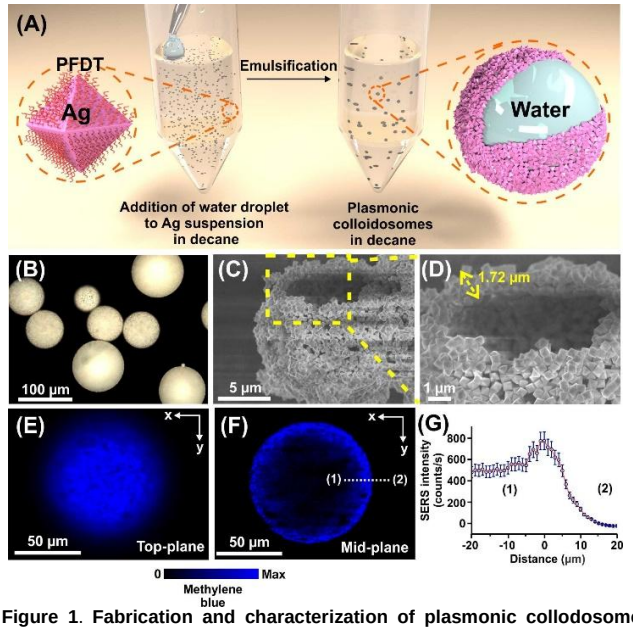

Figure 1. **Fabrication and characterization of plasmonic collodosomes** (A) Schematic illustration of the formation of plasmonic colloidosomes with PFDT-grafted Ag octahedral and their (B) microscopic images. SEM images of (C) a hollow colloidosome shell and (D) the magnified segment of the dash yellow box in (C). x-y SERS images of a colloidosome encapsulating methylene blue 10^{-6} M when laser is focused on its (E) top and (F) mid-plane. (G) SERS intensity-distance profile along the white dotted line of (F), from (1) to (2).

quantitative examination of the kinetics and molecular events occurring at the native interfacial reaction site.

Our *in-situ* SERS are performed with time-dependent x-y SERS imaging with laser focused on top of the colloidosome over 25 min (Figure 2C; Figure S4), aiming to investigate the reaction kinetics and molecular information. Briefly, colloidosomes encapsulating aqueous pH 1 or pH 7 solutions are immersed in a decane solution containing excess DY of 10^{-2} M. Control experiment using colloidosome in pH 7 exhibits only DY's C-N stretching mode at 1150 cm^{-1} over the entire reaction duration,[15] indicating no observable formation of HDY^+ (Figure 2C). Upon changing to pH 1 colloidosome, the SERS spectrum clearly exhibits the evolution of new vibrational features at 1283 and 1633 cm^{-1}, which are attributed to HDY^+'s N=N and C=C stretching modes, respectively.[15] The SERS image of a pH 1 colloidosome prior to the reaction only shows DY's 1150 cm^{-1} signal (yellow-indexed), whereas the SERS profiling of the same colloidosome after 15 minutes of reaction is overwhelmed by HDY^+ signature peak (red-indexed) at 1283 cm^{-1} (Figure 2D). This is attributed to the protonation of DY by H^+ at liquid-liquid interface to generate protonated HDY^+ ions which gradually penetrate from the interface into the encapsulated aqueous phase (pH 1; Figure S3). This also agrees with our control set-up involving bulk biphasic protonation of DY. Hence, we affirm the shell permeability of plasmonic colloidosome and exemplify its immense capability for compartmentalization of reactants to perform interfacial reactions involving the dynamic diffusion of molecules across the interface.

Plasmonic colloidosome also excels in the *in-situ* resolution of isomer structures in the reaction. We observe evident asymmetry in all the HDY^+ SERS features in pH 1 colloidosomes (Figure 3A, B).

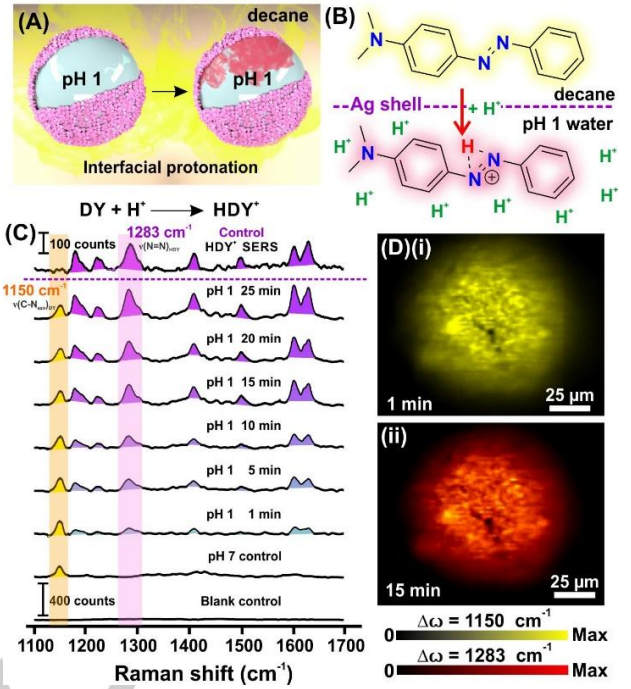

Figure 2. **Interfacial protonation of dimethyl yellow across the colloidosome shell**. (A) Schematic illustration of the interfacial protonation of dimethyl yellow (DY - yellow) to form protonated dimethyl yellow (HDY^+ - red) on colloidosomes encapsulating pH 1 solution. (B) Molecular scheme of the interfacial protonation of dimethyl yellow across the interface. (C) SERS spectrum obtained on colloidosomes encapsulating pH 1 submerged in DY 10^{-2} M solution in decane with time. Blank control refers to colloidosome encapsulating the same pH solution in pure decane. HDY^+ SERS spectrum was obtained with colloidal Ag solution. (D) SERS images of a colloidosome encapsulating pH 1 in dimethyl yellow solution at (i) 1 min and (ii) 15 min, with both DY's 1150 cm^{-1}(yellow-indexed) and HDY's 1283 cm^{-1} (red-indexed) signals are specified.

Generally, each asymmetric peak can be attributed to the presence of two contributing peaks (Figure 3A). In particular, the C-H waggingmode at 1180 cm^{-1} region comprises of 1178 and 1190 cm^{-1} peaks, the C-N stretching mode at 1220 cm^{-1} region comprises of 1220 and 1229 cm^{-1}, and the N=N stretching mode at 1283 cm^{-1} region comprises of 1281 and 1305 cm^{-1} signals (Figure 3A). These results reveal the presence of two isomeric products in DY protonation reaction with similar vibrational profiles that overlaps with each other. In combination with our density function theory (DFT) simulation results, we attribute this observation to the two major potential protonation sites in DY molecule, each of which situates at one of the N=N azo nitrogen atoms (red circles in Figure 3C), labelled as HDY^+(N1) and HDY^+(N2) accordingly, owing to their large coefficients in the two highest occupied molecular orbitals (HOMO; Figure S5A), also the most electron-rich atoms (Figure S5B), and possess strongest affinity to H^+ protons according to Pearson hard-soft acid-base theory.[16]

In addition, DFT simulation also affirms the protonation of DY's azo nitrogens to form isomeric HDY^+(N1) and HDY^+(N2) (Figure 3C), respectively. The simulated SERS spectra for both HDY^+ isomers demonstrate same characteristic vibrational modes of HDY^+ with slight differences in the vibrational energies: C-H wagging modes at 1204 and 1197 cm^{-1}, C-N stretching modes at 1249 and 1232 cm^{-1}, N=N stretching mode at 1320 and 1324 cm^{-1} for HDY^+(N1) and HDY^+(N2), respectively (Figure 3B, Table S3). This agreement with the

experimental spectrum clearly exemplifies the presence of both protonation isomeric products HDY^+(N1) and HDY^+(N2), which have not been resolved in literature SERS studies of this molecule.[15] Importantly, the normal Raman spectrum of HDY^+ (without the presence of any Ag particles) also exhibit identical peak asymmetry (Figure S7), which affirms that the asymmetry indeed arises from the presence of the two isomers of HDY^+, rather than from its different absorption configurations on Ag surface. The isomeric ratio analysis is performed using C-N stretching mode of HDY^+ in the 1220 cm^{-1} region, which comprises of two signals at 1220 and 1229 cm^{-1} which are assigned HDY^+(N2) and HDY^+(N1) isomer (Figure S6, Table S3), respectively. This feature is also located in a clear window free from DY SERS interference. Notably, we observe a constant relative contribution ratio of HDY^+(N2) / HDY^+(N1) at (1.5 ± 0.2) throughout the reaction time (Figure 3D). Such relative contribution ratio is also observed to be generally constant for other characteristic vibrational mode of HDY^+ (Figure S8). In fact, relative SERS contribution ratio is an excellent quantity to monitor the reaction progress.[17] The constant SERS contribution ratio indicates that the isomeric products of HDY^+ are directly formed in a thermodynamically-determined ratio from the start of reaction.[18] This can be vital in asymmetric synthesis where mixtures of isomeric products are common but remain indiscernible by chromatography techniques.[19] We also highlight the superiority of plasmonic colloidosome over HPLC technique, which is unable to resolve the above isomers with highly similar structures and physical properties (Figure S9).

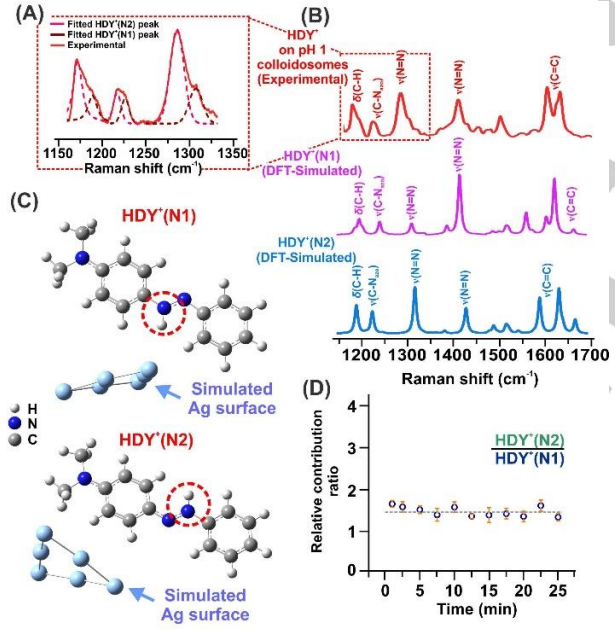

Figure 3. **Interpretation of SERS spectrum of DY and HDY^+, with likely molecular structures and interactions with Ag.** (A) Magnified spectrum of dotted region in the 'HDY^+ on pH 1 colloidosomes' spectrum in (B) with multiply-fitted peaks of two protonated isomers of HDY^+. (B) SERS spectra of HDY^+ observed on colloidosomes encapsulating pH 1 solution submerged in DY solution for 15 minutes, in comparison the DFT-simulated SERS spectra of both isomers of HDY^+. (C) Molecular structures of both isomers of HDY^+ with Ag-6 cluster (for SERS simulation) optimized by DFT-simulation. (D) Relative contribution ratio of fitted C-N stretching mode at 1220 cm^{-1} experimental peak in HDY^+ spectrum, with respect to time.

The capability of plasmonic colloidosome for the elucidation of critical reaction dynamic is further demonstrated by quantitatively investigating the temporal evolution of product HDY^+ *in-situ* at the liquid-liquid interface. We would like to emphasize that SERS intensity obtained at the shell is accurate for the kinetic modelling of the chemical species in both phases due to their fast diffusion rate over the ultrasmall droplet volume (see supporting information 3). Briefly, the overall reaction equation of DY's interfacial protonation are denoted in equation (1), respectively.

$$DY_{(org)} + H^+_{(aq)} \xrightarrow{k} HDY^+_{(aq)} \qquad (1)$$

where k is the rate constant of our model interfacial reaction.

We treat [DY] as a constant since there is a 10^6-fold excess of DY amount (2.5×10^{-5} mol) in the external organic phase compared to H^+ in the encapsulated aqueous phase (2.0×10^{-11} mol), as exemplified by the constant intensity of DY's C-N stretching SERS band (1150 cm^{-1}) of (1510 ± 160) counts (Figure S10). We also note that H^+ proton is Raman non-active, hence we use the SERS responses of HDY^+ for time-dependent profiling of H^+ consumption. The formation of HDY^+ product is tracked based on the relative intensity (R_t) of HDY^+ SERS signal (at 1283 cm^{-1}) compared to DY's constant SERS intensity (at 1150 cm^{-1}) at time t (equation 2). This is to minimize errors arising from experimental fluctuations.

$$R_t = \frac{I_{1283\,cm^{-1},t}}{I_{1150\,cm^{-1},t}} = \frac{\alpha_{HDY}[HDY^+]_t}{\alpha_{DY}[DY]} = c[HDY^+]_t \quad \text{, where } c = \frac{\alpha_{HDY}}{\alpha_{DY}[DY]} \qquad (2)$$

where α_{HDY} and α_{DY} (counts.L.mol^{-1}) are specific activity constants of HDY^+ and DY, respectively (see supporting information 3). To obtain $[H^+]$ necessary for the determination of k_{app}, we assume that all $[H^+]$ are consumed for the conversion of DY into HDY^+. Subsequently, we use the infinity quantity method to indirectly extract the consumption profile of H^+ concentration based on the production of HDY^+ (equation 3).[18]

$$c[H^+]_t = R_\infty - R_t = 4.6 - R_t \qquad (3)$$

where c denotes the proportionality constant in this relationship, which is proven to correlate with the aforementioned c in equation 2. R_∞ and R_t are the relative SERS intensity of HDY^+/DY at infinity time and time, t, respectively (Figure 4A). R_∞ remains constant at (4.6 ± 0.5) beyond 15 min (Figure 4A, B). Our derivation leads to the following relationship between ($4.6 - R_t$) in equation (4) of the reaction obeys first-order (reaction order is discussed in supporting information 3)

$$ln c[H^+] = ln(4.6 - R_t) = -k_{app}t + A \qquad (4)$$

where A= $ln\,[H^+]_0 + ln\,c$

Using equation (4), we indeed observe an evident linear relationship in the plot of $\ln(4.6 - R_t)$ against reaction time, t (Figure S12, supporting information 3), which verifies that the formation of HDY^+ obeys the 1st order kinetic with respect to H^+. Through the determination of its gradient in the plot for equation (4), the apparent rate constant (k_{app}) of our model interfacial reaction is determined to be 0.09 min^{-1}, which agrees with the value obtained at pH 2 (Figure S13; Supporting information 3). We also affirm the similar reaction kinetic using other vibrational modes of HDY^+ for reaction monitoring, such as the C=C stretching mode at 1633 cm^{-1} (Figure S14). Notably, we observe a consistent kinetic profiles by measuring the SERS spectra at half-plane of the colloidosome (Figure S15), which exemplifies the advantage of plasmonic colloidosome as a 3D SERS platform.

Additionally, plasmonic colloidosomes enable high throughput SERS monitoring of multiple interfacial reactions on colloidosomes. Colloidosomes encapsulating pH 1, pH 2 and pH 7 solutions are

monitored as isolated picoreactors in the same DY solution simultaneously but independently (Figure 4A, C). All colloidosomes response similarly to DY in the external phase (labelled yellow) and

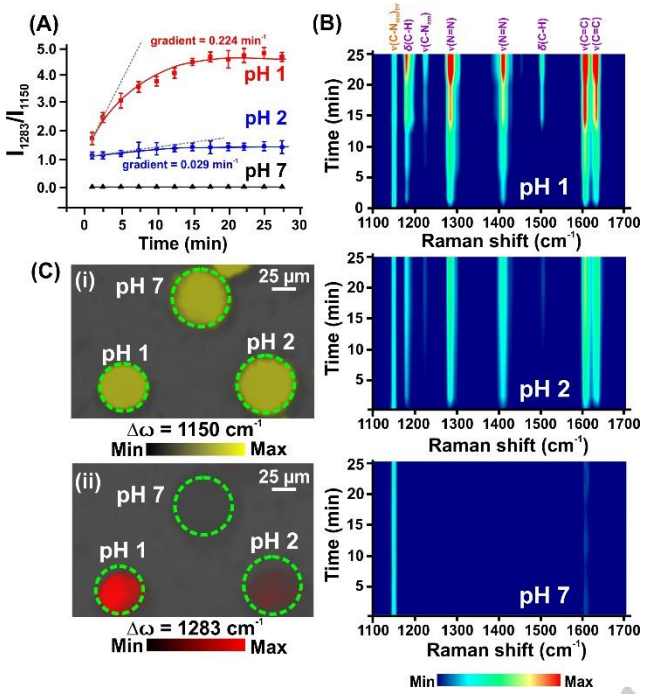

Figure 4. **The formation of HDY$^+$ at different pH**. (A) Area ratio of I_{1283}/I_{1150} peak and (B) time-resolved maps of the SERS spectra on the colloidosomes pH 1, pH 2 and pH 7 submerged in dimethyl yellow 10^{-2} M solution over time. (C) SERS images of a mixture of pH 1, pH 2 and pH 7 colloidosomes submerged in DY solution for after 15 minutes with (i) 1150 cm^{-1} (yellow-indexed) chosen and (ii) 1283 cm^{-1} (red-indexed) chosen. In the case of 1283 cm^{-1} shift, only the pH 1 colloidosomes exhibit strong signals, while pH 2 colloidosomes shows weak signals and pH 7 colloidosomes do not response to the shift.

exhibit uniform DY's 1150 cm^{-1} SERS intensities throughout the reaction (Figure 4B, C). Notably, pH 1 colloidosomes exhibit the steepest growth profile of HDY$^+$ signals (Figure 4B), which is also illustrated in our color-indexed SERS image where the pH 1 colloidosome is brightly lit when HDY$^+$ 1283 cm^{-1} signal is selected (labelled red, Figure 4C(ii)). Concurrently, pH 2 colloidosomes display a ~ 5-fold weaker red color intensity as observed in the same SERS image. We observe a ~ 10-fold slower initial formation rate of HDY$^+$ in pH 2 colloidosomes relative to pH 1 colloidosomes (initial gradients of R_I vs time plot of 0.224 min^{-1} and 0.029 min^{-1} respectively),[18] which obeys the previously determined first order kinetic of our model interfacial reaction (rate = $k_{app}[H^+]$; Figure 4A, S16). On the contrary, control pH 7 colloidosomes do not exhibit observable HDY$^+$ signals in the SERS spectrum and remain invisible in the SERS image of HDY$^+$ (Figure 4C(ii)). We also exclude errors resulting from crosstalking among closely-spaced plasmonic colloidosomes,[8] and also pH-induced effect on its Ag shell and SERS activities (Figure S17). Our results therefore emphasize on the importance of colloidosome's robustness to efficiently isolate reactions for high through-put reaction monitoring.

In conclusion, we have fabricated plasmonic colloidosomes from highly SERS active Ag octahedra, as a dual-phase picoreactor for simultaneous *in-situ* reaction monitoring and molecular analysis of liquid-liquid interfacial reaction. Applied in the decane-water interfacial protonation of dimethyl yellow on a < 200 pL droplet, our platform excels exemplifying the protonated isomers of HDY$^+$ in a constant thermodynamic ratio and the pseudo-first-order kinetic with the apparent rate constant of 0.09 min^{-1} of the reaction, as retrieved from *in-situ* SERS monitoring of the reaction progress. We also perform the parallel reaction monitoring with plasmonic colloidosomes, demonstrating their benefits as potential picoreactors for high through-put screening of reactions involving the multiple components soluble in both a single or two different phases. Therefore, plasmonic colloidosomes feature multiple advantages as a SERS microplatform for small-scale study of interfacial phenomena commonly encounter in the areas of food chemistry, clinical analysis and drug treatment.

Keywords: colloidosome • picoreactor • isomer identification • multiplex • in situ SERS • high through-put

[1] A. D. Dinsmore, M. F. Hsu, M. G. Nikolaides, M. Marquez, A. R. Bausch, D. A. Weitz, *Science.* **2002**, *298*, 1006-1009.
[2] Z. Wang, M. C. M. van Oers, F. P. J. T. Rutjes, J. C. M. van Hest, *Angew. Chem. Int. Ed.* **2012**, *51*, 10746-10750.
[3] M. Li, R. L. Harbron, J. V. M. Weaver, B. P. Binks, S. Mann, *Nat. Chem.* **2013**, *5*, 529-536.
[4] aS. Crossley, J. Faria, M. Shen, D. E. Resasco, *Science.* **2010**, *327*, 68-72; bK. Piradashvili, E. M. Alexandrino, F. R. Wurm, K. Landfester, *Chem. Rev.* **2016**, *116*, 2141-2169.
[5] R. Ameloot, F. Vermoortele, W. Vanhove, M. B. J. Roeffaers, B. F. Sels, D. E. De Vos, *Nat. Chem.* **2011**, *3*, 382-387.
[6] aC. Huo, M. Li, X. Huang, H. Yang, S. Mann, *Langmuir.* **2014**, *30*, 15047-15052; bC. Vázquez-Vázquez, B. Vaz, V. Giannini, M. Pérez-Lorenzo, R. A. Alvarez-Puebla, M. A. Correa-Duarte, *J. Am. Chem. Soc.* **2013**, *135*, 13616-13619.
[7] L. Liang, D. Huang, H. Wang, H. Li, S. Xu, Y. Chang, H. Li, Y.-W. Yang, C. Liang, W. Xu, *Anal. Chem.* **2015**, *87*, 2504-2510.
[8] G. C. Phan-Quang, H. K. Lee, I. Y. Phang, X. Y. Ling, *Angew. Chem. Int. Ed.* **2015**, *54*, 9691-9695.
[9] Z. Y. Bao, D. Y. Lei, R. Jiang, X. Liu, J. Dai, J. Wang, H. L. W. Chan, Y. H. Tsang, *Nanoscale.* **2014**, *6*, 9063-9070.
[10] aY.-F. Huang, M. Zhang, L.-B. Zhao, J.-M. Feng, D.-Y. Wu, B. Ren, Z.-Q. Tian, *Angew. Chem. Int. Ed.* **2014**, *53*, 2353-2357; bX. Wang, J.-H. Zhong, M. Zhang, Z. Liu, D.-Y. Wu, B. Ren, *Anal. Chem.* **2016**, *88*, 915-921.
[11] aL.-P. Wang, A. Titov, R. McGibbon, F. Liu, V. S. Pande, T. J. Martínez, *Nat. Chem.* **2014**, *6*, 1044-1048; bH. Ko, S. Singamaneni, V. V. Tsukruk, *Small* **2008**, *4*, 1576-1599.
[12] W. Fan, Y. H. Lee, S. Pedireddy, Q. Zhang, T. Liu, X. Y. Ling, *Nanoscale.* **2014**, *6*, 4843-4851.
[13] W. Gregory, J. M. Sanders, *Handbook of Organic Chemistry: For the Use of Students*, A. S. Barnes & Company, **1857**.
[14] D. Shechter, H. L. Dormann, C. D. Allis, S. B. Hake, *Nat. Protoc.* **2007**, *2*, 1445-1457.
[15] R. A. Ando, N. P. W. Pieczonka, P. S. Santos, R. F. Aroca, *Phys. Chem. Chem. Phys.* **2009**, *11*, 7505-7508.
[16] R. G. Pearson, *J. Chem. Educ.* **1968**, *45*, 581.
[17] W. Xie, B. Walkenfort, S. Schlücker, *J. Am. Chem. Soc.* **2013**, *135*, 1657-1660.
[18] P. Atkins, J. de Paula, *Atkins' Physical Chemistry*, OUP Oxford, **2010**.
[19] Y. Wang, Z. Yu, W. Ji, Y. Tanaka, H. Sui, B. Zhao, Y. Ozaki, *Angew. Chem. Int. Ed.* **2014**, *53*, 13866-13870.

Entry for the Table of Contents

COMMUNICATION

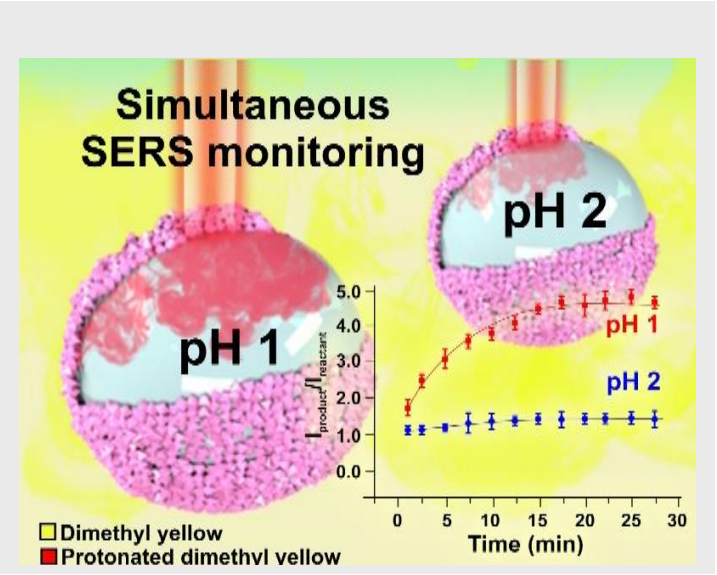

*Gia Chuong Phan-Quang, Hiang Kwee Lee, Xing Yi Ling**

Page No. – Page No.
Isolating Reactions at the Picoliter-scale: Parallel Control of Reaction Kinetics at the Liquid-liquid Interface .

Isolating & Monitoring Molecules at Picoliter Scale: Colloidosomes with Ag octahedra assembled at the water-in-decane emulsion interface is used as a pico-reactor capable of isolating the interfacial protonation of dimethyl yellow. Parallel SERS monitoring of multiple reactions can also be simultaneously performed during the reaction to identify reaction isomers and kinetics.

Experimental Section

Chemicals. Silver nitrate (≥ 99 %), anhydrous 1,5-pentanediol (PD, ≥ 97 %), poly(vinyl pyrrolidone) (PVP, average MW = 55,000); 1H,1H,2H,2H-perfluorodecanethiol (PFDT, ≥ 97 %), 4-methylbenzenethiol (4-MBT, ≥ 98%), decane (anhydrous, > 99%), methylene blue (MB, ≥ 82 %), and dimethyl yellow (DY, analytical standard, ≥ 98%) were purchased from Sigma Aldrich; copper (II) chloride (≥ 98 %) was from Alfa Aesar; ethanol (ACS, ISO, Reag. Ph Eur) was from EMSURE®; toluene (BAKER ANALYZED® A.C.S. Reagent) was from Avantor; propan-2-ol (HPLC grade) was from Fisher Scientific. All chemicals were applied without further purification. Milli-Q water (> 18.0 MΩ. cm) was purified with a Sartorius Arium® 611 UV ultrapure water system.

Synthesis and purification of silver nanocubes. The preparation of silver (Ag) octahedra was carried out based on the polyol method described in literature, first starting with the intermediate Ag nanocubes.[1] 10 mL PD solutions of $CuCl_2$ (8 mg/mL), PVP (20 mg/mL) and $AgNO_3$ (20 mg/mL) were prepared separately by sonication and vortex. 35 µL $CuCl_2$ solution was added to the $AgNO_3$ solution. 250 µL PVP precursor was added dropwise every 30 s while 500 µL $AgNO_3$ precursor was injected every min using a quick addition to a 10 minute-preheated 20 mL PD solution. The addition was continued until the mixture turned orange brown, followed by the further addition of 30 ml of PVP (20 mg/mL) and $AgNO_3$ (40 mg/mL with 120 µL $CuCl_2$) (both precursors were separately prepared in PD). The reaction was allowed to proceed until the precursors were used up. For the purification, PD was first removed by washing the mixture with acetone followed by ethanol. The suspension was then dispersed in 10 mL ethanol and 100 mL aqueous PVP solution (0.2 g/L) and filtered using Durapore® polyvinylidene fluoride filter membranes (Millipore) with pore sizes ranging from 5000 nm,

650 nm, 450 nm, several times for each pore size. SEM imaging was performed, from which the edge lengths of 250 Ag octahedra were measured and analyzed using ImageJ software.

Functionalization of Ag octahedra with perfluorodecanethiol. 50 mg of purified Ag octahedra were immersed in 10 mL of 1:1 propan-2-ol (IPA)/ethanol solution containing 0.1 mM of 1H,1H,2H,2H-perfluorodecanethiol (PFDT) for 6 h at room temperature. The colloidal suspension was then washed with copious amounts of ethanol, and subsequently dispersed in 1.0 mL of 1:1 IPA/ethanol.

Preparation of colloidosomes. 5 µL ultrapure water was added to 200 µL decane suspension containing 0.75 mg perfluorodecanethiol-functionalized Ag octahedra (referred to as Ag from this point onwards). Colloidosomes were formed by emulsification via vigorous shaking.

SERS characterization of colloidosomes. Methylene blue (3.2 mg/mL, 10^{-2} M) was prepared in aqueous solution using ultrapure water. Serial dilutions were performed to give a series of concentrations, ranging from 10^{-3} M to 10^{-12} M.

For SERS detection involving 20× (N.A. 0.45) objective lens, the as-prepared plasmonic colloidosomes were dispensed onto a 3 × 3 mm silicon substrate and submerged in 2.5 mL decane. The laser was focused at the top and edge of single colloidosomes. Both the colloidosome formation and SERS imaging for different analytes and concentrations were performed at least thrice to ensure the reproducibility of the SERS signal. All SERS intensities and spectra were obtained by averaging at least 20 individual spectrum.

For normal Raman evaluation of various analytes, Raman spectra were collected using the 20× (N.A. 0.45) objective lens from 0.5 µL of the respective analyte solution, with 100 s exposure time. Raman intensities and spectra were obtained by averaging at least 20 individual spectrum.

SERS analysis of Dimethyl yellow protonation and diffusion. The plasmonic colloidosomes prepared with aqueous solution with varying pH were dispensed onto a 3 × 3 mm silicon substrate and submerged in 2.5 mL decane solution of 10^{-2} M dimethyl yellow (DY). The laser was focused at the top of single colloidosomes. SERS imaging was performed at 2.5 minute interval over a period of 30 minutes. Both the colloidosome formation and SERS imaging were performed at least thrice to ensure the reproducibility of the SERS signal. All SERS intensities and spectra were obtained by averaging at least 20 individual spectrum.

SERS spectrum of protonatated dimethyl yellow : The SERS spectrum using was done using 0.01 mg of perfluorodecanethiol-grafted Ag octahedra dispersed in 0.5 mL of HDY^+ 10^{-3} M. The SERS imaging were performed at least thrice to ensure the reproducibility of the SERS signal. All SERS intensities and spectra were obtained by averaging at least 20 individual spectrum.

Density functional theory (DFT) simulation. The calculation of DY and HDY^+ on Ag surface were carried out using the unrestricted B3LYP exchange-correlation functional, as implemented in the Gaussian 09 computational chemistry package. The 6-31g (d) basis set was used for all atoms except Ag, for which the LANL2DZ basis set was employed. The Ag surface was modeled using an Ag-6 cluster.

Material characterization. SEM imaging was performed with JEOL-JSM-7600F microscope and QX-102 capsules.[2] UV-vis spectroscopic measurements were conducted with a Cary 60 UV-Vis spectrometer. Microscopic images were taken with Olympus BX51 microscope under 10× (0.30 BD) objective lens. SERS measurements were performed using both x-y and x-z imaging mode of the Ramantouch microspectrometer (Nanophoton Inc, Osaka, Japan) with an excitation wavelength of 785 nm. When using 20× (N.A. 0.45) objective lens, laser power was set at 1100.5 μW with 10 s

accumulation time (unless otherwise stated) for data collection between 200 cm^{-1} to 1800 cm^{-1}. All SERS spectra and intensities were obtained by averaging at least 20 individual spectra from each SERS image. High performance liquid chromatography (HPLC) was performed with Shimadzu SDP-20A, with MeOH/Acetonitrile gradient dilution over 40 minutes, and dual detection wavelengths at 435 nm.

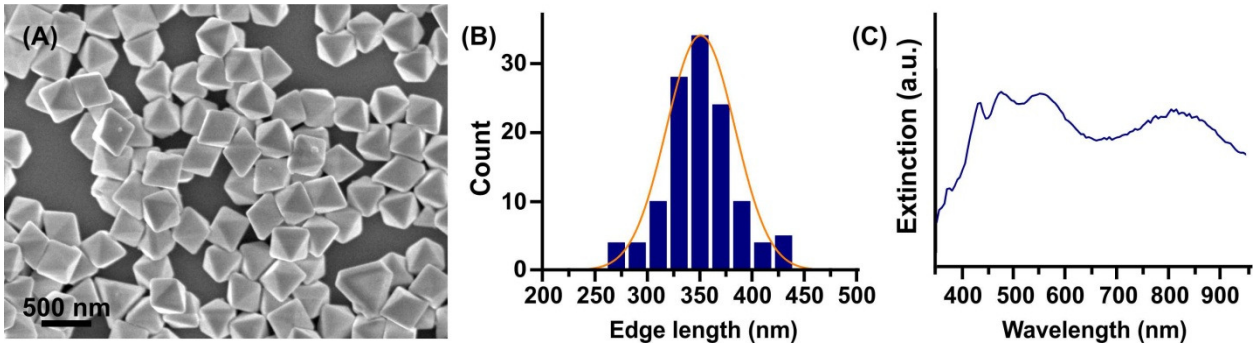

Figure S1. Characterization of Ag octahedra. (A) SEM image of as-synthesized Ag octahedra and (B) its size distribution. (C) Extinction spectrum of colloidal Ag octahedra. The peaks in the 400 - 600 nm window are assigned as hexapole and higher order resonances and the broak peak at ~ 810 nm is assigned as quadrupole resonance.[1b]

Table S1. SERS band assignments of methylene blue

SERS band (cm^{-1})	Band assignment.[3]
456	C-N-C deformation
503	C-N-C deformation
1406	C-H in plane ring deformation
1446	C-N stretching
1633	Ring C-C stretching

Supporting information 1: Determination of SERS enhancement factor of Ag-octahedra plasmonic colloidosomes.

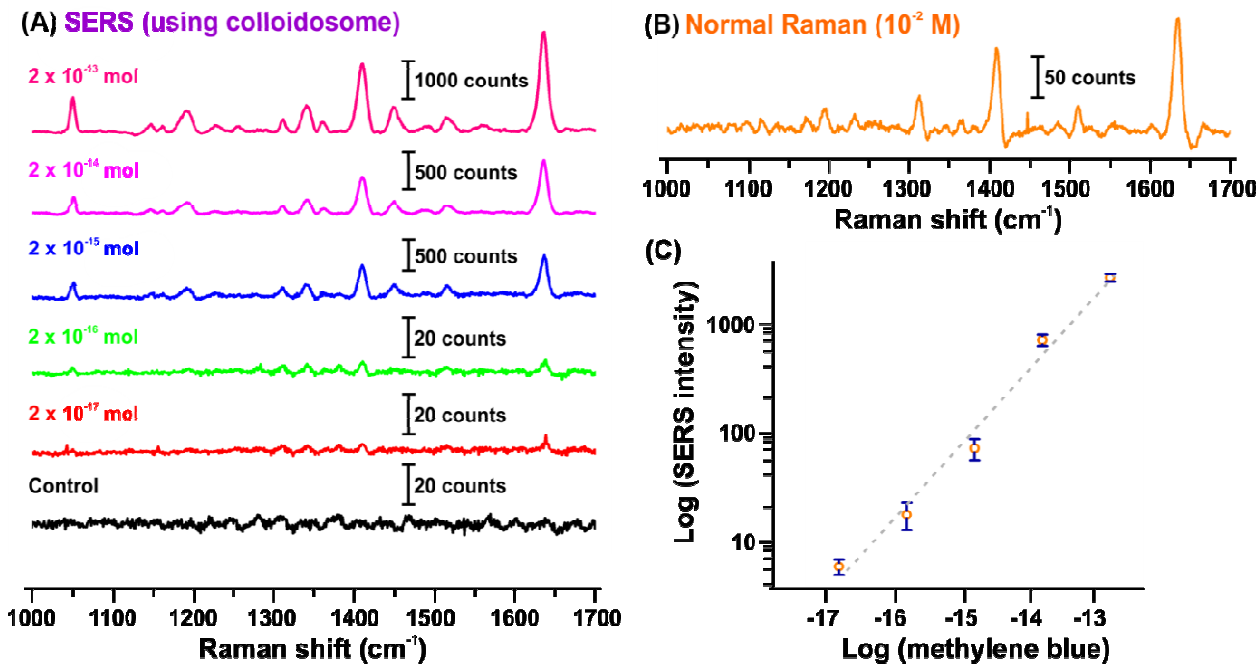

Figure S2. (A) SERS spectra and (B) normal Raman spectrum (200s exposure time) of methylene blue obtained using colloidosomes, and water droplet respectively. (C) SERS intensity of the 1633 cm^{-1} signal methylene blue encapsulated in plasmonic colloidosomes with concentration ranging from 20 amol to 0.2 pmol. Control refers to blank colloidosomes in the absence of methylene blue.

SERS measurements are conducted on single colloidosomes with diameter of (72 ± 20) μm, or volume of ~195 pL. For example, a single colloidosome encapsulating 10^{-7} M methylene blue solution contains ~ 2×10^{-17} mole methylene blue. We report the methylene blue concentration in its actual mole number to emphasize on the ultratrace amount of analyte that can be detected with plasmonic colloidosome platform.

With reference to the 1633 cm^{-1} SERS band, we calculate the analytical enhancement factor of methylene blue detection as followed:

$$\text{Analytical EF} = [(I_{SERS}) / (I_{Raman})] \times [(C_{Raman}) / (C_{SERS})]$$

$$= [(7/10) / (122 / 200)] \times (10^{-2} / 10^{-7})$$

$$= 10^{5}$$

where N_{SERS} and N_{Raman} are the corresponding concentrations measured using plasmonic colloidosomes (10^{-7} M; 2×10^{-17} mol encapsulated as per colloidosome) and normal Raman of methylene blue (10^{-2} M), respectively. I_{SERS} and I_{Raman} are the time-normalized intensities measured using SERS and normal Raman, respectively, at their corresponding concentration.

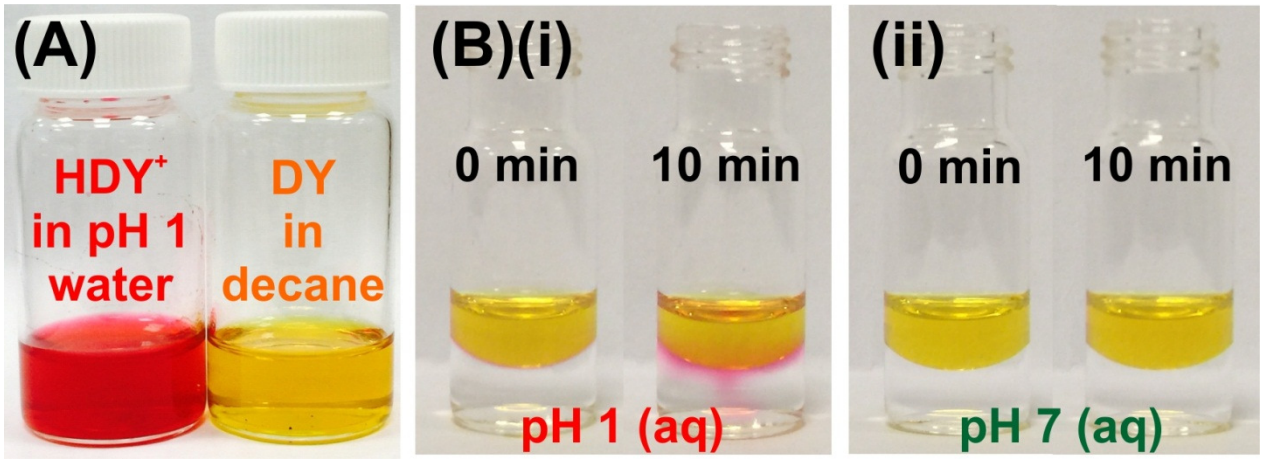

Figure S3. (A) HDY^+ 10^{-2} M solution in aqueous pH 1 solution and DY 10^{-2} M solution in decane. Neutral DY form is only soluble in organic decane solvent and while charged HDY^+ form is soluble in acidic aqueous solution. (B) Protonation and diffusion of DY across the decane-water interface performed in conventional two-phase system: (i) formation of HDY^+ in the aqueous phase when pH 1 is used and (ii) no observable reaction when pH 7 is used. The two forms of dimethyl yellow are characterized by distinct optical characteristics, namely the different maximum absorption wavelengths at 435 nm and 515 nm, for DY and HDY^+, respectively. [4]

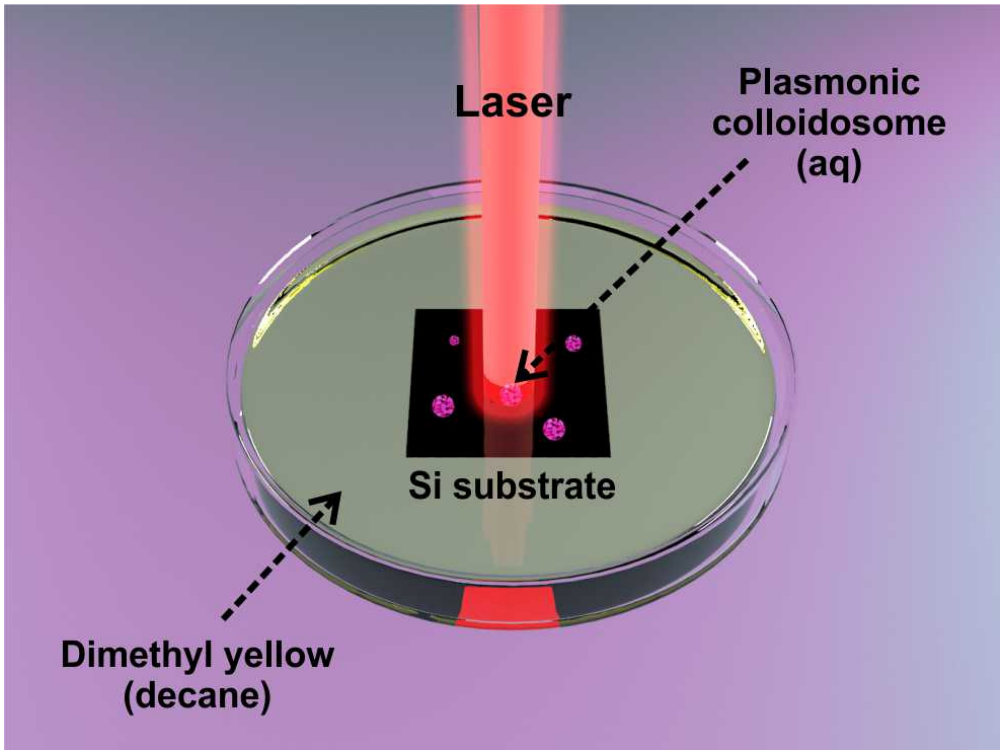

Figure S4. Schematic of experimental set-up for the *in situ* SERS monitoring of interfacial protonation of dimethyl yellow (in external decane phase) with plasmonic colloidosomes (encapsulating aqueous H^+ solution).

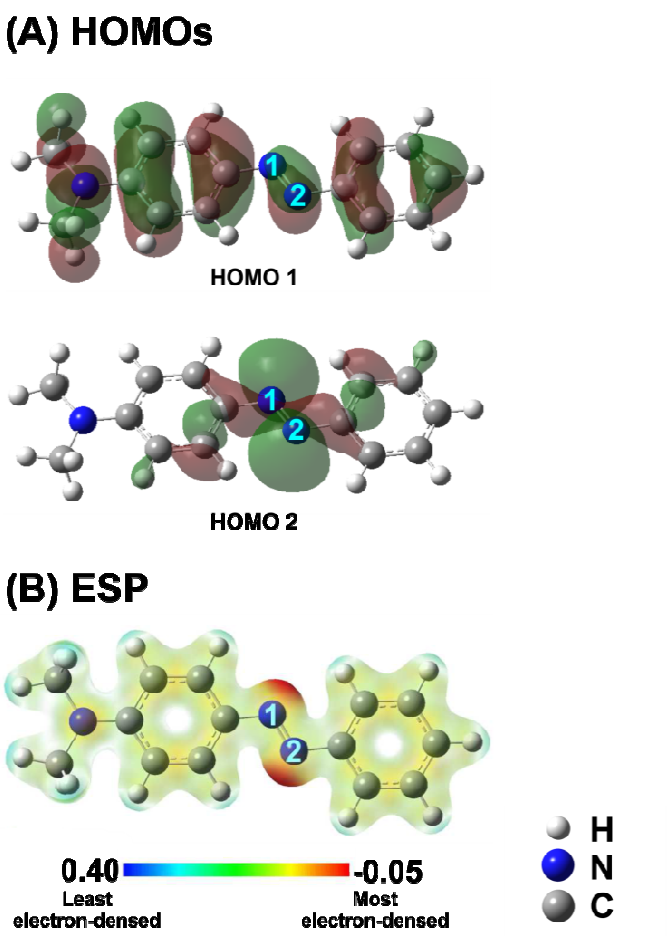

Figure S5. (A) Molecular representation of the two highest energy HOMOs of DY molecule, where the azo group contributes high coefficients in. (B) Electrostatic potential map of DY molecule. The red dash-box highlights the N=N azo group.

Table S2. SERS band assignments of dimethyl yellow (DY)

Experimental SERS band (cm^{-1})	DFT-Simulated SERS band (cm^{-1})	Band assignment.[4-5]
1150	1183	C-N_{azo} stretching
1202	1233	C-N_{azo} stretching
1415	1477	N=N stretching
1604	1643	Ring C-C stretching

Table S3. SERS band assignments of protonated dimethyl yellow (HDY^+)

Experimental SERS band (cm^{-1})	DFT-Simulated SERS band of HDY^+(N1) (cm^{-1})	DFT-Simulated SERS band of HDY^+(N2) (cm^{-1})	Band assignment.[4-5]
1180	1204	1197	C-H wagging
1220	1249	1237	C-N_{azo} stretching
1283	1320	1324	N=N stretching
1410	1423	1440	N=N stretching
1604	1634	1644	Ring C-C stretching
1633	1671	1680	Ring C-C stretching

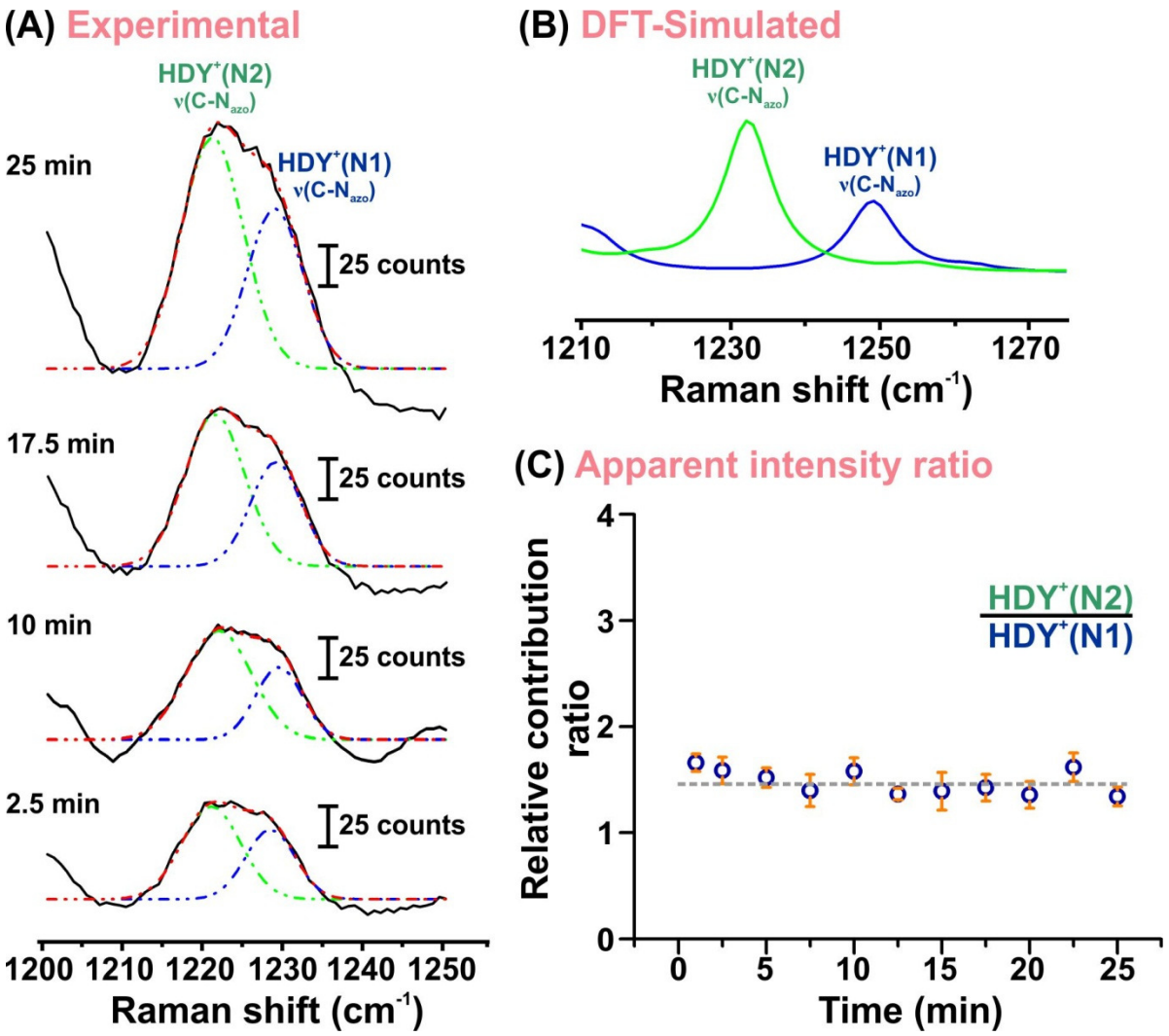

Figure S6. (A) Fitted HDY^+(N2) and HDY^+(N1) C-N stretching modes within experimental 1220 cm^{-1} peak in time-resolved HDY^+ spectra. (B) DFT-Simulated C-N stretching modes of HDY^+(N2) and HDY^+(N1). (C) Relative SERS contribution ratio of fitted C-N stretching peaks for HDY^+(N2)/HDY^+(N1) in 1220 cm^{-1} experimental peak in HDY^+ spectrum, with respect to time.

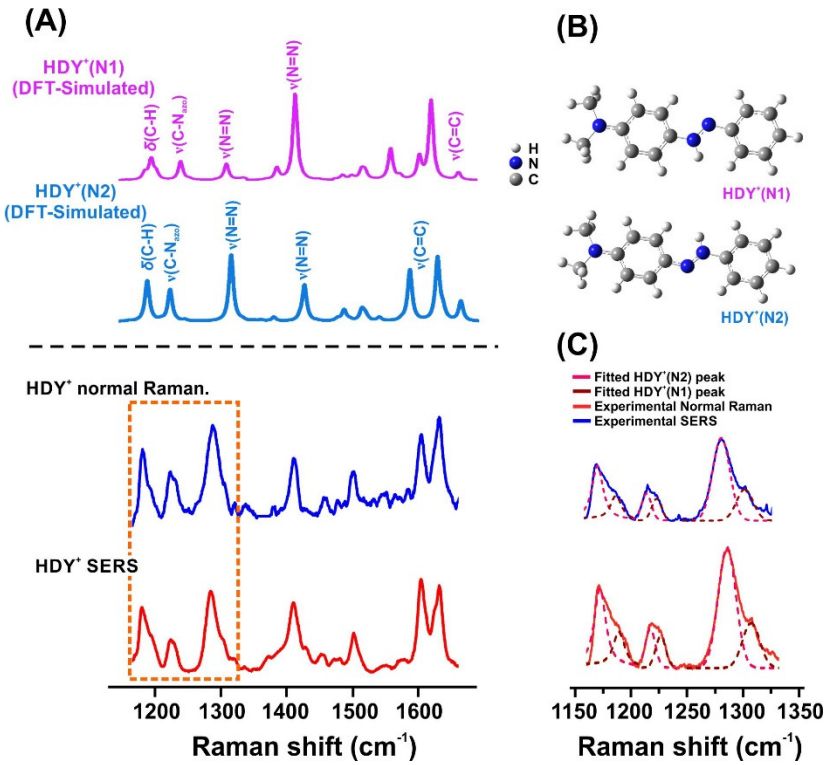

Figure S7. (A) Comparison of HDY^+ SERS spectrum and normal Raman spectrum, with DFT-simulated spectra. (B) DFT-optimized molecular structures of the isomers. (C) Zoom-in segment of the dotted-box region in (A) and the peak fit analysis of the 1180, 1220 and 1283 cm^{-1} vibrational bands observed in both SERS and normal Raman.

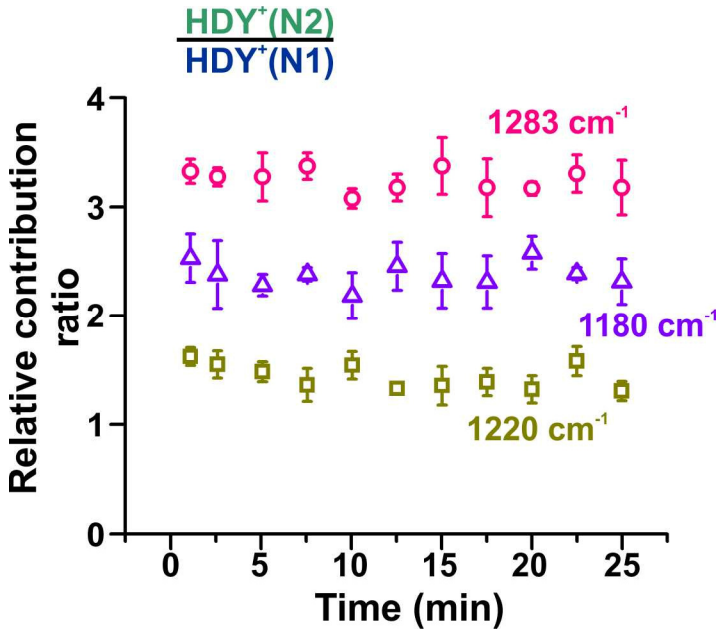

Figure S8. Relative SERS contribution ratio for HDY^+(N2)/HDY^+(N1) analyzed in 1180, 1220 and 1283 cm^{-1} experimental peaks in HDY^+ spectrum, with respect to time. The difference in the apparent ratio values is attributed to the difference in the Raman activity and Raman cross section of different vibrational modes.[6]

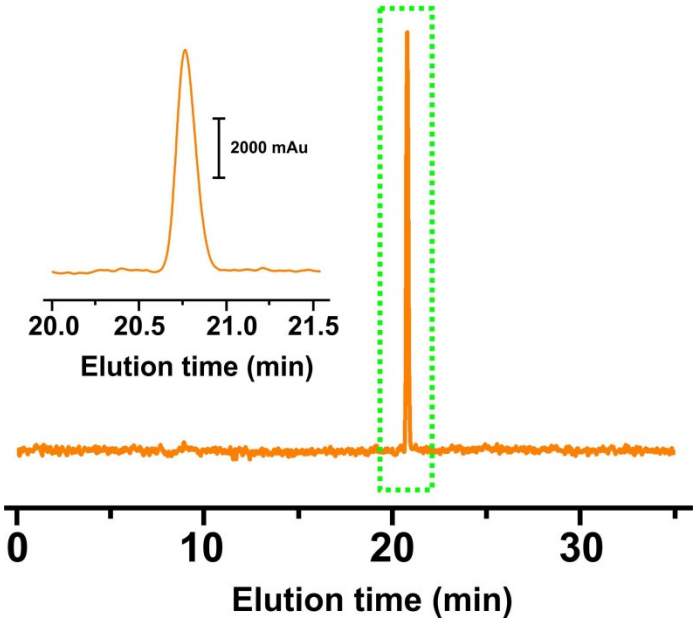

Figure S9. High performance liquid chromatography (HPLC) elution profile and the zoom-in signal of HDY^+ observed at 20.80 min (MeOH/ACN gradient elution, detection wavelength 435 nm). It is impossible to resolve the two isomers in the peak due to their highly similar polarity.

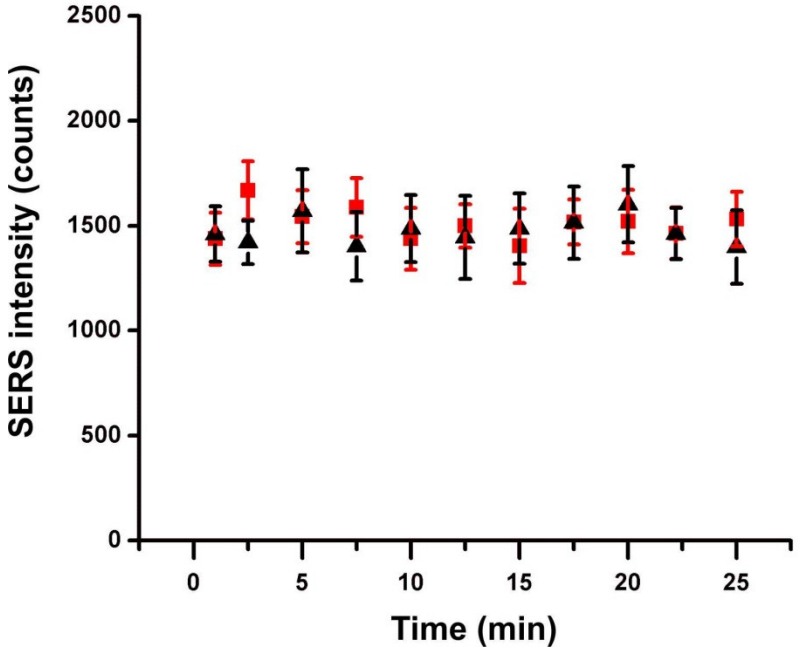

Figure S10. Area intensity of DY's 1150 cm^{-1} signal with time, on colloidosomes pH 1 (red) and pH 7 (black). This also highlights the advantage of our stable SERS platform over existing colloidal systems in SERS monitoring, where the latters are prone to large signal fluctuations due to aggregation effect over time.[7] In fact, our plasmonic colloidosome has demonstrated its signal stability and reproducibility owing to the precedently assembled Ag shell skeleton.[8]

Supporting information 2. Use of DY as the reference.

Our reaction is performed with plasmonic colloidosomes submerged in the bulk organic phase containing DY 10^{-2} M solution (**Figure S4**). We observe a constant SERS intensity (1510 ± 160 counts) of DY signals, namely the 1150 cm^{-1} peak when colloidosomes of both pH 1 and pH 7 are used in the reaction. Hence, we use the above signal as a reference to standardize the evolution of the HDY^+ signals (I_{1283}/I_{1150}) in our kinetic calculation. The observation may be due to the excess amount of DY molecules as compared to the H^+ ions in the plasmonic colloidosomes, and the diffusion of excess DY to replenish the reacted DY at the interface is fast enough to maintain signal stability within our exposure time of 10s.[9]

- Mole number of DY in the external phase :

$$n_{DY} = [DY] \times V_{org} = 10^{-2} M \times 2.5\, mL = 2.5 \times 10^{-5}\, mol$$

- Mole number of H^+ in a plasmonic colloidosome :

$$n_{H+} = [H^+] \times V_{cldsome} = 10^{-1} M \times 195\, pL = 1.95 \times 10^{-11}\, mol$$

Therefore, DY is in 10^6-fold excess in comparison to H^+ amount, and hence its concentration in the organic phase is insignificantly affected during the course of reaction.

Supporting information 3. Reaction kinetics.

The capability of plasmonic colloidosome for the elucidation of critical reaction dynamic is further demonstrated by quantitatively investigating the temporal evolution of product HDY^+ *in-situ* at the liquid-liquid interface. We observe that SERS intensity obtained at the colloidosome shell (at the decane-water interface) is able to accurately reflects the concentration of analytes in the bulk of both the inner aqueous phase and external organic phase due to the fast diffusion of the dye molecules to the interface. This is illustrated by the consistent DY 1150 cm^{-1} intensity obtained at the interface throughout the course of reaction (Figure S10), resulting from its high and constant bulk phase concentration, and also due to the fast diffusion of excess DY to replenish the reacted DY at the interface, which maintains signal stability within our exposure time of 10 s.[9] The same explanation is also applicable for the other species HDY^+ in the aqueous phase where it can diffuse over the entire encapsulated capsule fast enough, such that the SERS signals observed at the Ag shell to be representative of its amount in the whole vessel. More importantly, HDY^+ in the internal aqueous phase can diffuse at a much greater rate due to the ultrasmall volume of < 200 pL of our vessel. In particular, small picoliter droplets allow up to 8 orders of magnitude faster rate of diffusion and homogenization as compared to bulk vial-based solution, according to the following formula of diffusion rate in liquid system: [10]

$$t \approx {r^2}/{D}$$

(t is diffusion time required for droplet homogenization, r is droplet diameter, D is diffusion coefficient of the analyte)

Hence, we perform the kinetic calculation based on the SERS intensity observed at the colloidosome shell which can accurately reflect the amount of reactants and products in both phases.

Briefly, the overall reaction equation and the rate equation of DY's interfacial protonation are denoted in equation (1) and (2), respectively.

$$DY_{(org)} + H^{+}{}_{(aq)} \xrightarrow{k} HDY^{+}{}_{(aq)} \quad (1)$$

$$rate\ of\ equation\ (v) = -\frac{d[H^{+}]}{dt} = k[H^{+}]^{n}[DY]^{m} \quad (2)$$

where k is the rate constant of our model interfacial reaction, $[H^+]$ and [DY] are the concentrations of H^+ and DY, respectively, while n and m are integers representing the rate order of H^+ and DY, respectively.

We did attempt to quantify the concentration HDY^+ in the water phase, by isolating HDY^+ in plasmonic colloidosomes to obtain an intensity-concentration calibration curve similar to the methylene blue case. However, our colloidosome preparation procedure involves an intense emulsification step which facilitates the diffusion of the encapsulated HDY^+ to the external decane phase as DY molecules, according to the equilibrium $DY_{(org)} + H^+_{(aq)} \rightleftharpoons HDY^+_{(aq)}$. Even though the inner aqueous phase contains pH 1 solution which minimize the formation of DY, we still observe a great amount of DY diffused to the decane phase (both physically and via SERS measurement in Figure S10), which we attribute to the concentration gradient difference. Hence, we are unable to estimate the actual concentration of the HDY^+ remained within the colloidosomes for quantification. Nevertheless, we are able to retrieve the kinetics based on the monitoring of the SERS intensity of HDY^+ signals, with correlation to the stable DY signal from the excess DY in the organic phase. Such methodology of reaction monitoring based on solely SERS intensity without correlation to the actual concentration is indeed proven to be an accurate and reliable technique to investigate reaction kinetics.[7b] Hence, we are confident that our analysis based on SERS intensity monitoring genuinely reflects the kinetics of this reaction.

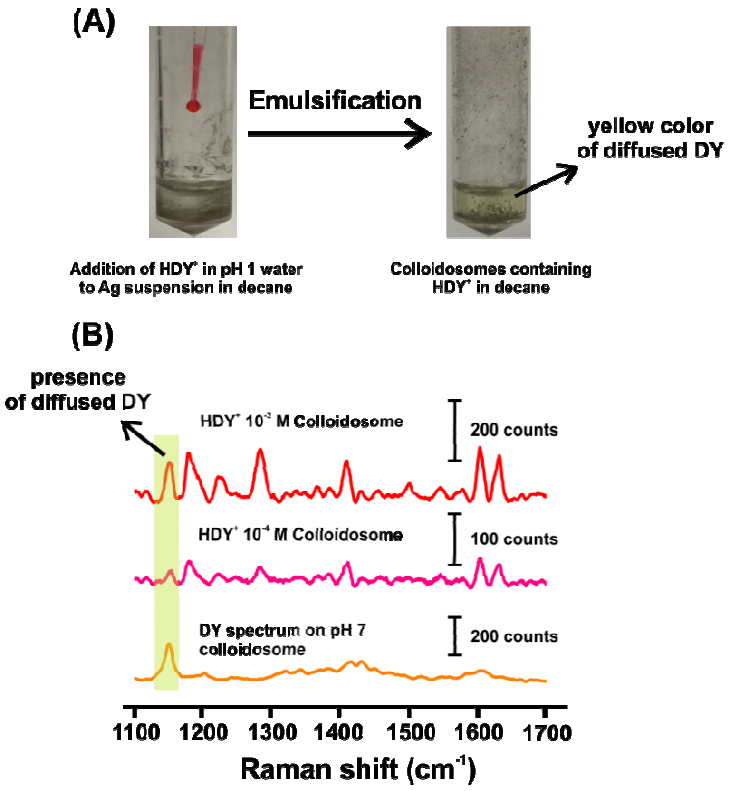

Figure S11. Diffusion of DY to the external phase as shown by (A) digital images of the vials before and after emulsification and formation of colloidosomes. Even though HDY^+(red) is originally dissolved in water, the intense emulsification step facilitates the formation of DY (yellow) and its diffusion to the decane phase. (B) SERS spectra measured on colloidosomes sample prepared with HDY^+ 10^{-3} M and 10^{-4} M, with the control of DY spectrum. The DY's 1150 cm^{-1} mode is always present, which proves the difficulties in the isolation of HDY^+ in the colloidosomes.

We treat [DY] as a constant since there is a 10^6-fold excess of DY amount (2.5×10^{-5} mol) in the external organic phase compared to H^+ in the encapsulated aqueous phase (2.0×10^{-11} mol), as exemplified by the constant intensity of DY's C-N stretching SERS band (1150 cm^{-1}) of (1510 ± 160) counts (Figure S9). Together with the assumption of n = 1 (to be verified later), we can therefore rewrite equation (2) into a pseudo 1st order reaction as simplified in equation (3).

$$-\frac{d[H^+]}{dt} = k[H^+]^n[DY]^m$$

$$-\frac{d[H^+]}{dt} = k_{app}[H^+]^n \quad \text{, where } k_{app} = k[DY]^m \tag{3}$$

where k and k_{app} represents the intrinsic and apparent rate constant, respectively, *t* is the time from the start of reaction and [DY] is a constant.

By integrating the pseudo 1st order rate law (equation 3), we obtain the 1st order integrated rate law as described in equation (4)

$$[H^+] = [H^+]_o e^{-k_{app}t}$$

$$ln[H^+] = -k_{app}t + ln[H^+]_o \tag{4}$$

where $[H^+]_o$ is the initial concentration of H^+ at t = 0 min.

We note that H^+ proton is Raman non-active and uses the SERS responses of HDY^+ instead for latter time-dependent profiling of H^+ consumption. $[HDY^+]$ is directly proportional to the SERS intensity of its characteristic SERS band at 1283 cm^{-1} according to the relationship in equation 5. We

track the formation of HDY^+ product based on the relative intensity of its SERS signal compared to DY's constant SERS intensity at 1150 cm^{-1} (equation 6). This is to eliminate the possibility of any intensity change arising from random fluctuation of our experimental set-up instead.

$$I_{1283\,cm^{-1},t} = a_{HDY}[HDY^+]_t \quad (5)$$

$$R_t = \frac{I_{1283\,cm^{-1},t}}{I_{1150\,cm^{-1},t}} = \frac{a_{HDY}[HDY^+]_t}{a_{DY}[DY]} = c[HDY^+]_t \quad \text{, where } c = \frac{a_{HDY}}{a_{DY}[DY]} \quad (6)$$

where α_{HDY} and α_{DY} (counts.L.mol^{-1}) are specific activity constants of HDY^+ and DY, respectively. Such activity constant is commonly used to relate the SERS intensity of chemical species with their concentration; it is a comprehensive term comprising of contribution from laser intensity, the effective molecular SERS cross-section of the corresponding vibrational mode, and experimental conditions including the sample temperature and the solvent diffraction constant.[6] These aforementioned factors, and therefore α_{HDY} and α_{DY}, are essentially constant as all the experimental conditions for our SERS measurements are precisely controlled to ensure their consistency.

To obtain $[H^+]$ necessary for the determination of k_{app}, we assume that all $[H^+]$ are consumed for the conversion of DY into HDY^+. Subsequently, we use the infinity quantity method to indirectly extract the consumption profile of H^+ concentration.[11] Infinity quantity method is a powerful technique to relate product formation profile to the reactant consumption, which state that the difference in a physical quantity of the product at time infinity (∞) and a specific time (*t)* from the onset of reaction is directly proportional to the reactant concentration (equation 7).

$$R_\infty - R_t = c[HDY^+]_\infty - c[HDY^+]_t = c[H^+]_t \quad (7)$$

(derivation below)

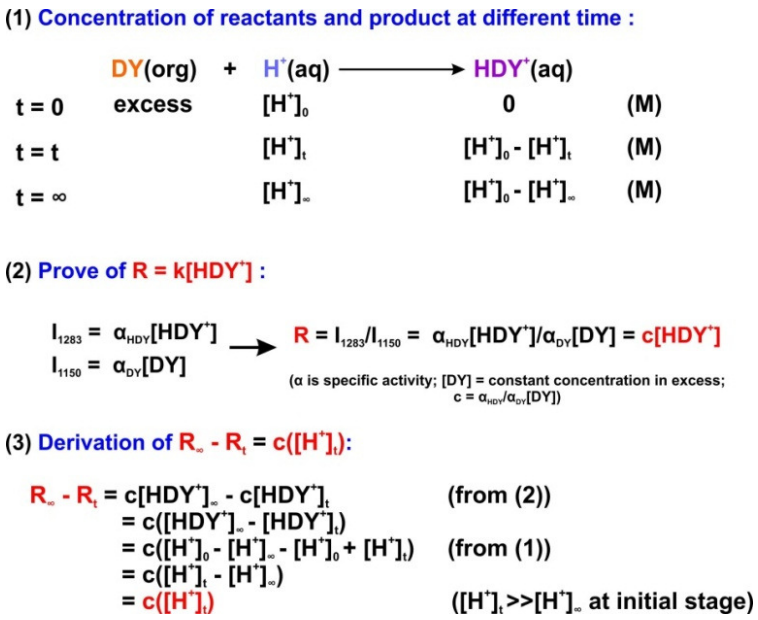

where *c* denotes the proportionality constant in this relationship, which is proven to correlate with the aforementioned *c*. R_∞ can be obtained from the plateau value of the relative SERS intensity (R)-time plot, which exhibits an initial incremental growth of SERS intensity that eventually remained constant at (4.6 ± 0.5) beyond 15 min (Figure 4A, B). Consequently, R_∞ = (4.6 ± 0.5) and equation (7) can be simplified as followed:

$$c[H^+]_t = 4.6 - R_t \quad (8)$$

By substituting equation (8) into equation (4),

$$ln[H^+] = -k_{app}t + ln[H^+]_0$$

$$ln[H^+] + lnc = -k_{app}t + ln[H^+]_0 + lnc$$

$$ln(c[H^+]) = -k_{app}t + A \quad , where\ A = ln[H^+]_0 + lnc$$

$$ln(4.6 - R_t) = -k_{app}t + A \qquad (9)$$

Using equation (9), we note an evident linear relationship in the plot of ln(4.6 – R_t) against reaction time, *t* (Figure S10A). The presence of such linear relationship therefore verify that the interfacial protonation of DY obeys the 1st order kinetic, where the formation of HDY^+ is only dependent on the concentration of H^+. Through the determination of its gradient in the plot for equation (9), the apparent rate constant (k_{app}) of our model interfacial reaction is determined to be 0.09 min^{-1}. Notably, the apparent rate constant derived at pH 1 is also in agreement with the value obtained at pH 2 (0.09 min^{-1}; Figure S11).

To confirm the order of the reaction, we also perform the profiling of $1/c[H^+]$ vs. time (equation 10) according to the integrated rate law of second-order reaction :

$$1/[H^+] = k_{app}t + 1/[H^+]_0$$

$$1/c[H^+] = k_{app}t/c + 1/c[H^+]_0$$

$$1/(4.6 - R_t) = k_{app}t/c + A' \quad where\ A' = 1/c[H^+]_0 \qquad (10)$$

We do observe that the plot of $1/c[H^+]$ or 1/(4.6 – R_t) vs. time does not produce a linear plot (Figure S10B). Hence, it affirms that the reaction indeed obeys the first-order kinetics (as determined above) and not second-order.

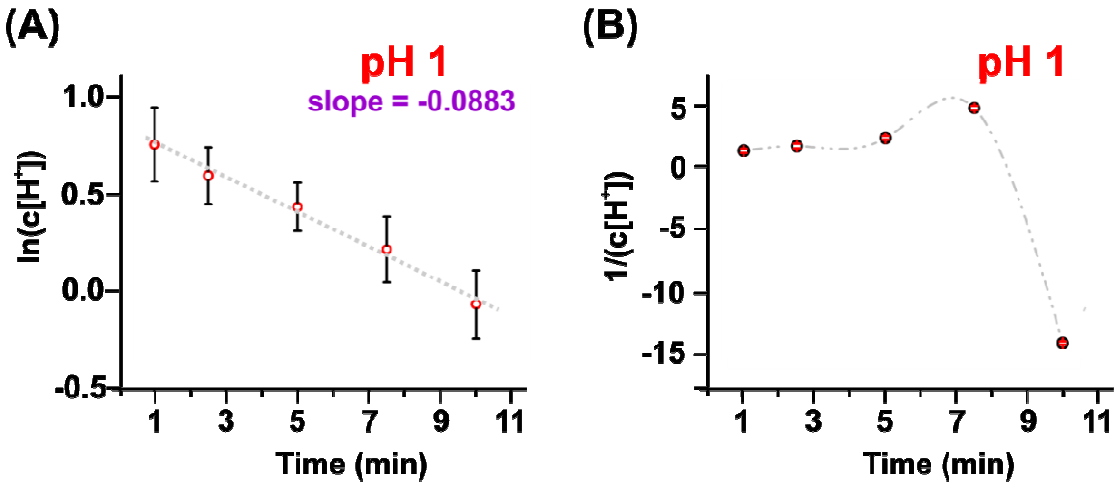

Figure S12. Plot of (A) ln(c[H^+]) vs time and (B) 1/c[H^+] vs time in the reaction on pH 1 colloidosome.

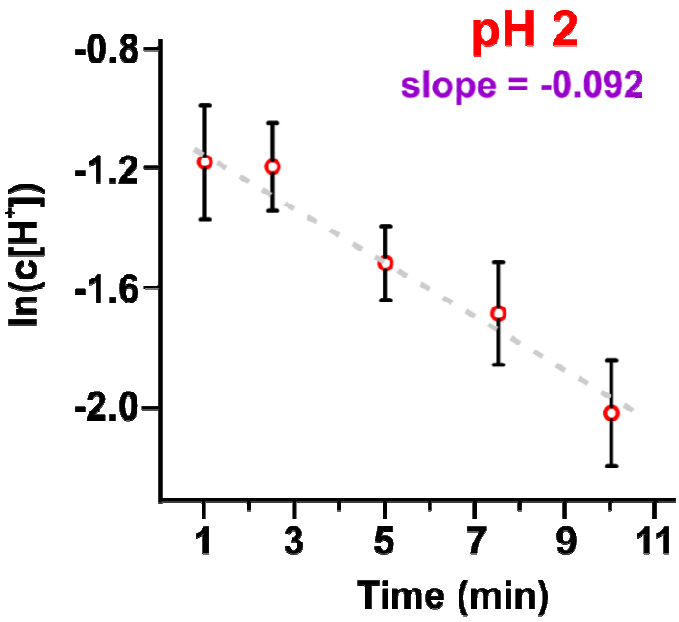

Figure S13. Plot of ln(c[H^+]) vs time in the reaction on pH 2 colloidosome.

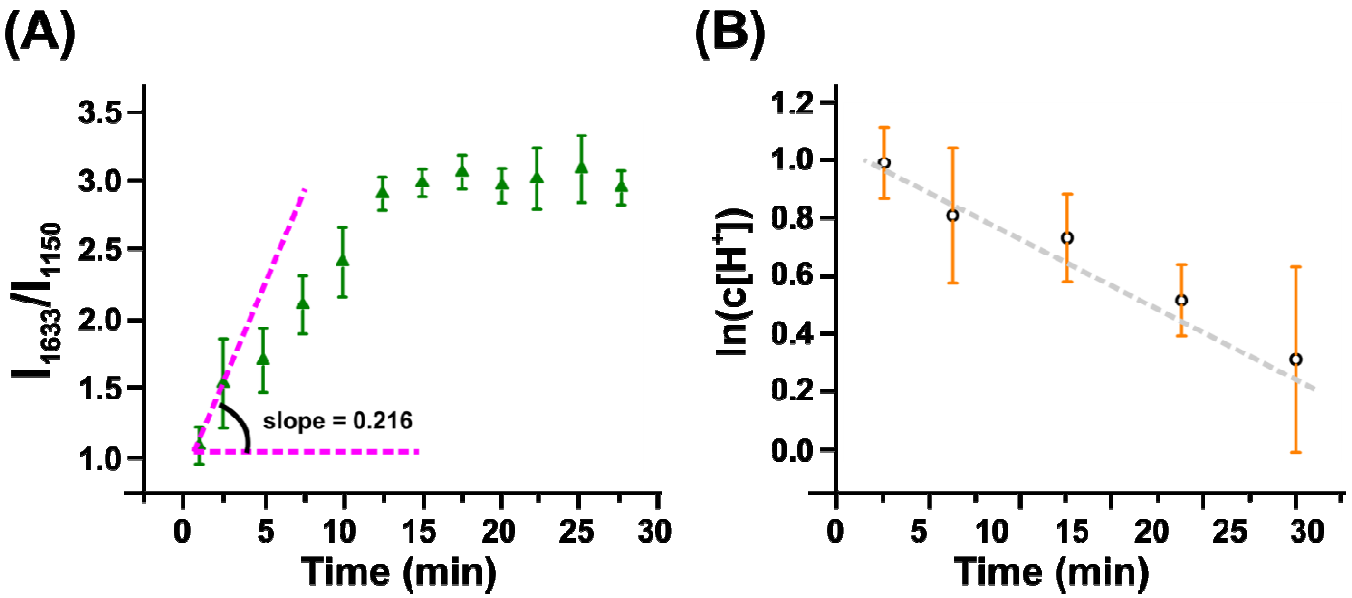

Figure S14. Reaction monitoring using HDY^+ 1633 cm^{-1} peak. (A) Area ratio of HDY's 1633 cm^{-1} peak and DY's 1150 cm^{-1} peak on the pH 1 colloidosomes submerged in decane over time. (B) Plot of $\ln(c[H^+])$ vs time in the reaction on pH 1 colloidosome.

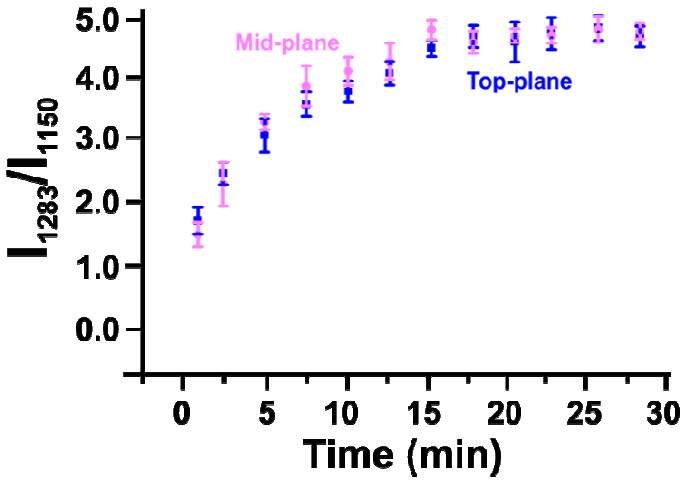

Figure S15. Similar growth profile of HDY^+ formation based on I_{1283}/I_{1150} ratio obtained on colloidosome with laser focused on top- and mid-plane.

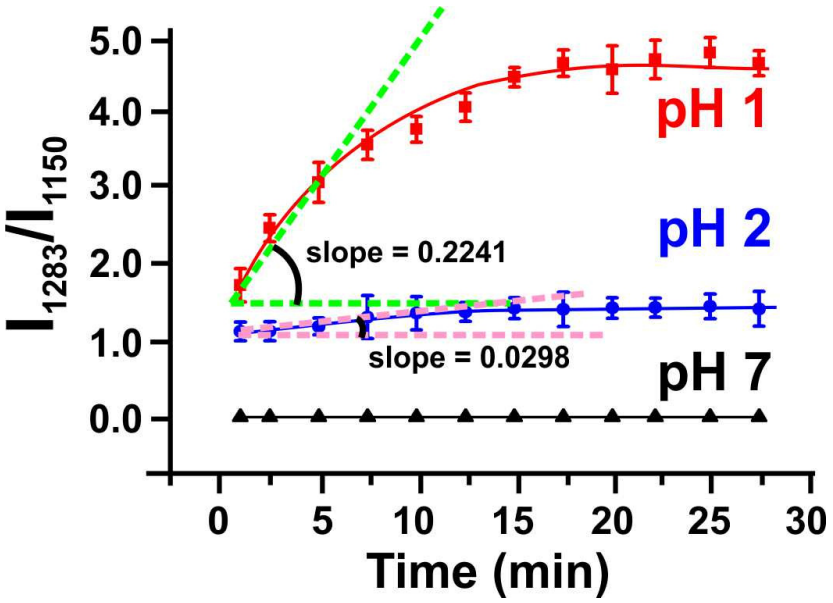

Figure S16. Initial rate analysis of the HDY^+ formation observed on colloidosome pH 1 and pH 2.

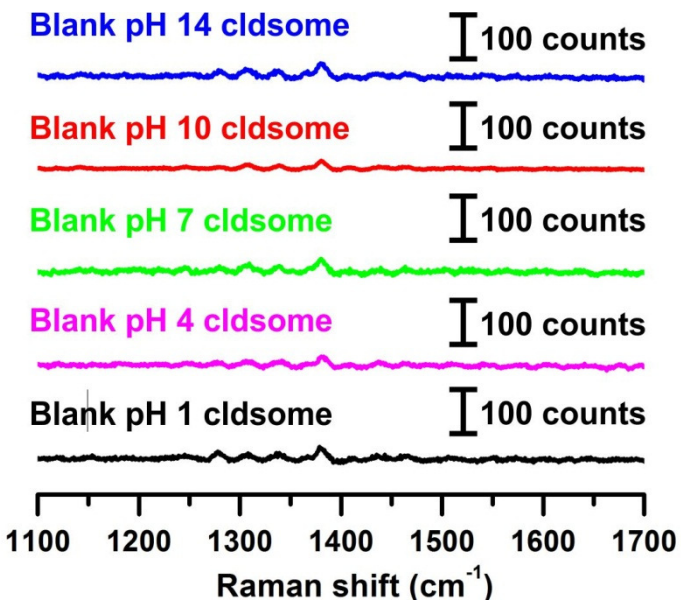

Figure S17. SERS background of blank colloidosomes encapsulating pH 1 to pH 14.

REFERENCES

1. (a) Mulvihill, M.; Tao, A.; Benjauthrit, K.; Arnold, J.; Yang, P., Surface-Enhanced Raman Spectroscopy for Trace Arsenic Detection in Contaminated Water. *Angew. Chem. Int. Ed.* **2008,** *47* (34), 6456-6460; (b) Tao, A.; Sinsermsuksakul, P.; Yang, P., Polyhedral Silver Nanocrystals with Distinct Scattering Signatures. *Angew. Chem. Int. Ed.* **2006,** *45* (28), 4597-4601.
2. Dyab, A. K. F.; Paunov, V. N., Particle stabilised emulsions studied by WETSEM technique. *Soft Matter* **2010,** *6* (12), 2613-2615.
3. (a) Lee, H. K.; Lee, Y. H.; Phang, I. Y.; Wei, J.; Miao, Y.-E.; Liu, T.; Ling, X. Y., Plasmonic Liquid Marbles: A Miniature Substrate-less SERS Platform for Quantitative and Multiplex Ultratrace Molecular Detection. *Angew. Chem.* **2014,** *126* (20), 5154-5158; (b) Xiao, G.-N.; Man, S.-Q., Surface-enhanced Raman scattering of methylene blue adsorbed on cap-shaped silver nanoparticles. *Chem. Phys. Lett.* **2007,** *447* (4–6), 305-309.
4. Ando, R. A.; Pieczonka, N. P. W.; Santos, P. S.; Aroca, R. F., Chromic materials for responsive surface-enhanced resonance Raman scattering systems: a nanometric pH sensor. *Phys. Chem. Chem. Phys.* **2009,** *11* (34), 7505-7508.
5. Zhang, Z. L.; Mo, Y. J., The pH Dependence of the SERS 38 Spectra of Methyl Yellow in Silver Colloid. **2011,** *26* (6).
6. Ko, H.; Singamaneni, S.; Tsukruk, V. V., Nanostructured Surfaces and Assemblies as SERS Media. *Small* **2008,** *4* (10), 1576-1599.
7. (a) Shen, W.; Lin, X.; Jiang, C.; Li, C.; Lin, H.; Huang, J.; Wang, S.; Liu, G.; Yan, X.; Zhong, Q.; Ren, B., Reliable Quantitative SERS Analysis Facilitated by Core–Shell Nanoparticles with Embedded Internal Standards. *Angew. Chem. Int. Ed.* **2015,** *54* (25), 7308-7312; (b) Xie, W.; Walkenfort, B.; Schlücker, S., Label-Free SERS Monitoring of Chemical Reactions Catalyzed by Small Gold Nanoparticles Using 3D Plasmonic Superstructures. *J. Am. Chem. Soc.* **2013,** *135* (5), 1657-1660.
8. Phan-Quang, G. C.; Lee, H. K.; Phang, I. Y.; Ling, X. Y., Plasmonic Colloidosomes as Three-Dimensional SERS Platforms with Enhanced Surface Area for Multiphase Sub-Microliter Toxin Sensing. *Angewandte Chemie* **2015,** *127* (33), 9827-9831.
9. Darby, B. L.; Le Ru, E. C., Competition between Molecular Adsorption and Diffusion: Dramatic Consequences for SERS in Colloidal Solutions. *J. Am. Chem. Soc.* **2014,** *136* (31), 10965-10973.
10. (a) Gratzl, M.; Yi, C., Diffusional microtitration: acid/base titrations in pico- and femtoliter samples. *Anal. Chem.* **1993,** *65* (15), 2085-2088; (b) Okhonin, V.; Wong, E.; Krylov, S. N., Mathematical Model for Mixing Reactants in a Capillary Microreactor by Transverse Diffusion of Laminar Flow Profiles. *Anal. Chem.* **2008,** *80* (19), 7482-7486.
11. (a) Atkins, P.; de Paula, J., *Atkins' Physical Chemistry*. OUP Oxford: 2010; (b) Harris, R. C.; Hultman, E., Kinetic methods that are independent of the rate of reaction. *Clin. Chem.* **1983,** *29* (12), 2079-81.